A&A 399, 1159–1166 (2003)
DOI: 10.1051/0004-6361:20021852

Astronomy & Astrophysics

X-ray and radio observations of the activation stages of an X-class solar flare

F. Fárník[1], H. S. Hudson[2], M. Karlický[1], and T. Kosugi[3]

[1] Astronomical Institute of the Academy of Sciences, 251 65 Ondřejov, Czech Republic
[2] University of California, Berkeley, USA
[3] ISAS, Sagamihara, Kanagawa, Japan

Received 8 July 2002 / Accepted 5 December 2002

Abstract. We report interesting developments prior to the impulsive phase of an X-class solar flare that occurred on September 24, 2001. Our multiwavelength study makes use of X-ray data from the *Yohkoh* satellite, the Ondřejov radio spectral observations in the decimetric band, and the new Hard X-Ray Spectrometer instrument (HXRS) on board the MTI satellite. The GOES time history of this event showed a "precursor" phase starting as early as two hours prior to the impulsive phase, and we have used various data sets to identify what parts of this development could be associated with the flare itself. The most interesting time interval was identified roughly one hour before the main peak when an unusual drifting radio continuum was observed together with two radio sources (at 327 and 164 MHz) in positions corresponding to expanding loops seen in *Yohkoh*/SXT and SOHO/EIT images, accompanied by a filament disappearence during the same period. Hard X-ray observations revealed a soft spectrum that we interpret as non-thermal, located within loop structures observed in soft X-rays along the magnetic neutral line. The hard X-ray emission continued for more than one hour, as observed in turn by the two spacecraft. In the initial phase of the flare itself, the hard X-ray emission arose in structures closely identifiable with the early soft X-ray loops, which appeared to evolve smoothly into the post-flare loop system of the flare maximum. The decimeter spectra showed loosely-correlated spiky emission at frequencies consistent with the densities inferred from soft X-rays, but with rapid drifts implying motions along field lines. From all these data we infer that the initiation of the flare involved non-thermal processes extending along the neutral line in the photosphere, systematically including open magnetic field lines as shown by the occurrence of interplanetary Type III bursts observed by the WAVES spectrometer on board the WIND spacecraft.

Key words. Sun: flares – Sun: X-rays, gamma-rays – Sun: radio radiation

1. Introduction

The initial development of a solar flare has long promised to provide information about the physical conditions in the corona that lead to a flare or coronal mass ejection (CME) (e.g., Gaizauskas 1989). The appearance of the soft X-ray light curve of a flare often suggests the presence of "preflare heating," or a "precursor" burst, and in the effort to predict flare occurrence many possible pre-flare indicators have been proposed. In general these have not passed statistical tests, and for the most part such manifestations cannot be distinguished from chance occurrence during enhanced activity (Tappin 1991). Theoretical work also frequently attempts to associate such a distinct phase with the gradual development of conditions that lead to the catastrophic development needed for flare energy release (e.g. Vršnak 1989).

The most detailed search with modern X-ray imaging data (Fárník & Savy 1998) did find some flare events in which the flaring loop appeared to brighten well before the impulsive phase of the flare (25% of a sample of 32 flares well-observed by *Yohkoh*). However there was no particular correlation found between the early brightenings and the flare properties, and so the authors concluded that there was "no definite evidence of a special "pre-flare" or "precursor" phase in solar flares". This result is consistent with that of Kahler (1979) and Webb (1985) based on the less-frequent sampling of the *Skylab* soft X-ray images; Webb stated rather clearly "The preflare feature was not at the flare site... There was no... correlation of preflare event characteristics with the subsequent flare energy". Nevertheless it is well-known that filament activations often precede the impulsive phase of a flare, or the acceleration time of a CME. This may seem inconsistent with the inconclusive searches for X-ray precursor activity, but one may presume that (a) most flares, especially less energetic ones, may not have an associated filament eruption; and/or (b) that the X-ray signatures sought for do not strongly accompany filament activation.

In this paper we report multiwavelength observations prior to an X-class flare which exhibited interesting preflare characteristics. At present we have no deep understanding of the reasons for flare or CME eruption. Two current classes of models include the "tether-cutting" (Moore & Roumeliotis 1992) and "breakout" (Antiochos et al. 1998) scenarios, as well as the idea of triggering by interacting bipole (e.g.,

Send offprint requests to: F. Fárník, e-mail: ffarnik@asu.cas.cz

Machado et al. 1988). Comprehensive observations of the pre-flare environment should help guide us to which (if either) of these pictures are helpful to our physical understanding.

The particular event we discuss occurred on 24 September 2001. As Fig. 1 shows, these observations reveal early X-ray increases as observed by the GOES 8 soft X-ray photometers. We have observed this early interval well with the instruments on *Yohkoh*, SOHO, and the new Hard X-ray Burst Spectrometer (Sect. 2), and also make use of Nançay radioheliograph images and Catania Hα data, plus Ondřejov, Tremsdorf, and WIND/WAVES radio spectra in the decimeter, meter, and hectometer ranges respectively. Figure 2 shows, for later reference, a roadmap to the image features based mainly on *Yohkoh*/SXT images (SXT = Soft X-ray Telescope) that we feel are important in the analysis.

2. Hard X-Ray Spectrometer (HXRS)

The HXRS instrument (built in the Czech Republic and launched as a secondary payload on the Multispectral Thermal Imager spacecraft (MTI) in March 2000) observes solar hard X-ray spectra as a function of time with two scintillation counters. Because data from HXRS have not often appeared in the literature yet, we provide some details here regarding the instrument's capabilities and its cross-calibration against HXT (Hard X-ray Telescope onboard *Yohkoh*) data (see also Fárník et al. 2001). HXRS is a scintillation-counter spectrometer with 8 energy bands covering the range 13–500 keV. Its unique feature is a gain-changing capability to allow it to respond to very large flares; this was not needed for the September 24, 2001 event discussed here. Its basic time resolution is 0.2 s, its effective area 4.5 cm^2 for each of two detectors, and its entrance window 1.02 mm Al. It also has an on-board radioisotope calibration source (Am^{241}).

3. Flare of September 24, 2001

3.1. GOES soft X-ray and hard X-ray chronology

Figure 1 indicates the times of *Yohkoh* SXT images and the soft X-ray flare development as observed by GOES-8. This flare has a striking early soft X-ray increase, starting about 09:20 UT, as early as an hour prior to the impulsive phase, and preceded by other activity. It is an excellent example of a major flare with what is normally called a gradual soft X-ray precursor, namely the ramp-up of GOES brightness commencing at about this time. For discussion we divide this time series into four parts, an early activation stage (prior to 09:20 UT), a second activation stage (until about 10:00 UT), and a third activation stage lasting until the impulsive phase begins at about 10:18 UT. In this paper we do not discuss the flare main phase (after GOES maximum at 10:40 UT) except to note the location of the bright arcade loops. In later sections we will show from various sources of data how these stages may be related to the overall flare development. As a first step in this process, we show the raw GOES temperature and emission measure profiles in Fig. 1. These are uncorrected for background and hence give no reliable quantitative information before the impulsive

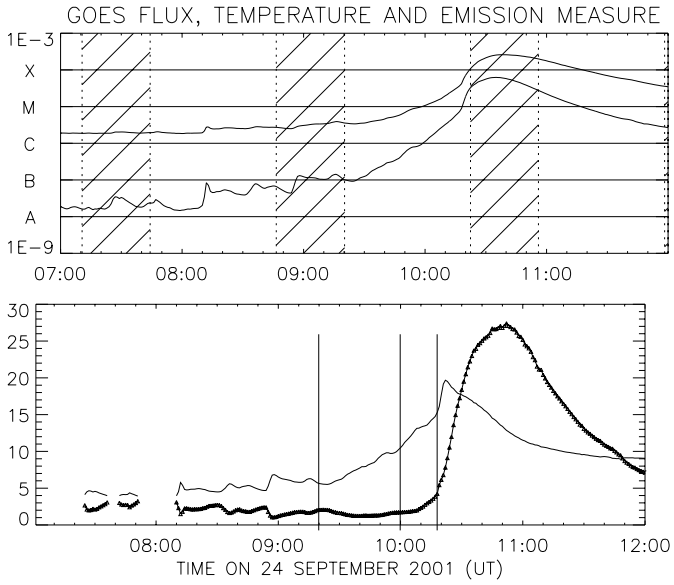

Fig. 1. Upper part: GOES 8 two-band fluxes plot; *Yohkoh* eclipse periods are shown with diagonal shading. Lower part: temperature (thin line) and emission measure (thick line) as derived from the GOES data. The *Y*-axis gives both the temperature (MK) and also the emission measure (10^{49} cm^{-3}). The temperatures and emission measures only give qualitative information, since no background has been subtracted. Thin vertical lines in the lower panel show how we have divided the development of this flare into four stages.

phase, but do show a steadily increasing apparent temperature during the activation stages (09:20 UT to 10:18 UT). These elevated apparent temperatures reflect the presence of energy release throughout this one-hour period.

The flare of 24 September 2001 (see Table 1) also had an extraordinarily long development as seen in hard X-rays, as expected from the Neupert effect (Dennis & Zarro 1993; Hudson & McKenzie 2000), because of the long soft X-ray rise phase. The initial phases of the flare chiefly interest us here, since almost no hard X-ray observations of early flare development have been reported. Figure 3 shows hard X-ray light curves for the activation stages of the flare, as observed by *Yohkoh* HXT, and Fig. 4 shows the late activation phase and impulsive phase via the HXRS data. Taken altogether the hard X-ray emission extends for more than one hour. The rapid variations seen in these early hard X-rays, and discussed below in the context of the decimeter variability, suggest the presence of particle acceleration. The detection of these variations in the three lowest energy bands of the HXT instrument, with its relatively large effective area, gives us an opportunity to estimate the spectrum during one of these events. We show the example near 10:04 UT in Fig. 6, with dashed lines showing estimates of the background level for each channel. In the case of the highest band (M2 at 33–53 keV) this background is close to the normal detector background, whereas for the lower channels there is a steadily increasing background which we attribute to loops filling with hot plasma and emitting soft X-rays thermally.

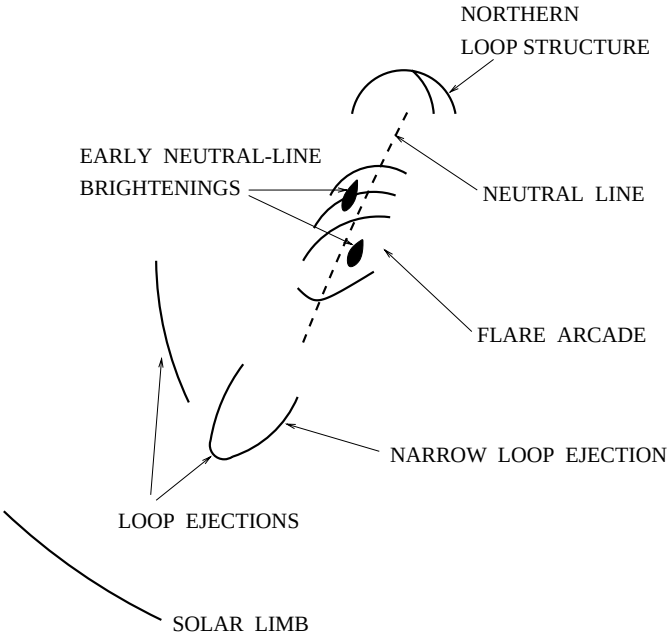

Fig. 2. "Roadmap" sketch showing the features discussed in the text. From SXT soft X-ray images (Sect. 3.2) we show the pre-flare active region, the later activation stage, and the flare loops. Items shown are called out in the text in boldface type. This sketch and all images in this paper are oriented with north up, east to the left.

Table 1. Flare parameters.

GOES class:	X2.6
H-alpha class:	2B
GOES times:	0930-1040-1139 UT
Location:	S16E23
NOAA region:	9632
Hard X-ray spectral index at 10:25 UT:	2.5

3.2. Soft X-ray imaging

Movies of SXT images, with different fields of view and exposure times, provide the main basis for our division of the flare into four stages. Please refer to Fig. 1 for the timing and Fig. 2 for the image roadmap, which shows the features discussed below (these are identified in the text by boldface type).

We also present in Fig. 7 three representative SXT views (09:48 UT, 10:13 UT, and 11:01 UT) of the flare "precursor" and the flare itself. During the first development stage, ending at about 09:20, the SXT data have relatively poor coverage. Useful whole-Sun images at 08:19, 08:27, 08:35, 08:44 UT are the only material with which we can study the first activation stage. These images show brightening along the **neutral line** in the time range 08:27:20 UT to 08:44:24 UT, followed by brightening in the **northern loop structure**. The soft X-ray difference images in Fig. 5 show these developments.

During the second development stage (from 09:20 UT) the soft X-ray images show additional phenomena that could also be related to the flare eruption. Unfortunately the image cadence remains poor until 09:45:52 UT, when flare mode

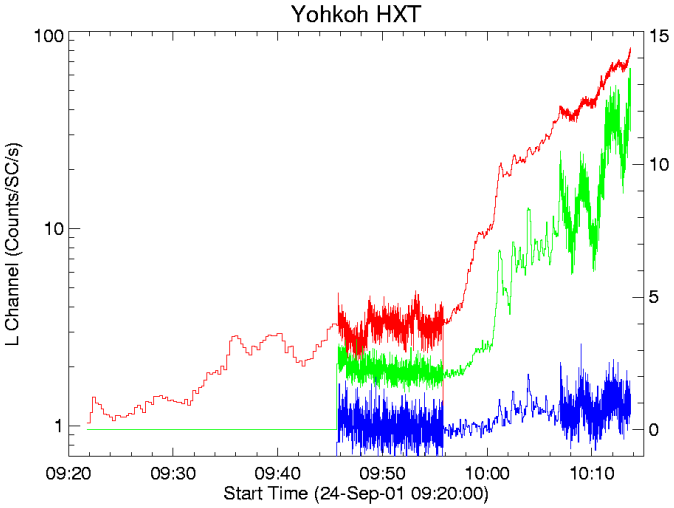

Fig. 3. *L*, *M*1 and *M*2 energy bands of *Yohkoh*/HXT showing fluxes from the second stage of the flare. Higher-energy bands are not available prior to about 09:46 UT because *Yohkoh* did not enter Flare mode until then; following that the thin sections of the light curves show where *Yohkoh* telemetry only ran in Medium rate, with a reduced soft X-ray image cadence.

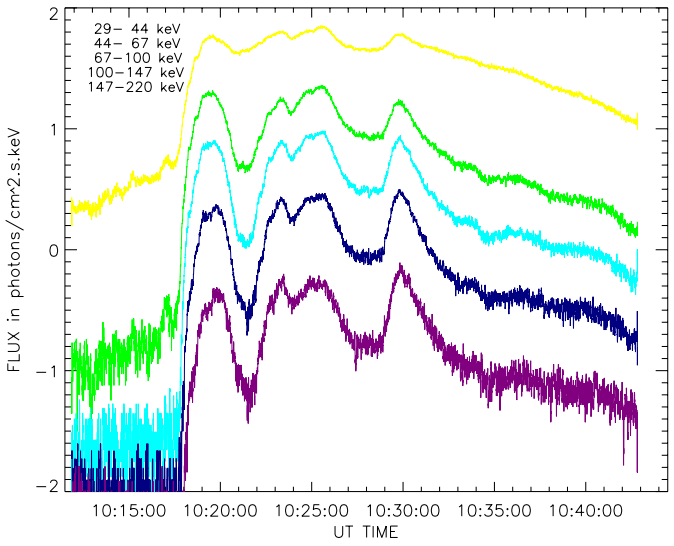

Fig. 4. Hard X-ray observations of the flare of 24 September 2001, showing data from the Hard X-ray Burst Spectrometer on board the MTI satellite. The plot shows fluxes in five energy bands as defined in the upper left corner.

triggered. The brightening in the **northern structure** could be observed in the image at 09:24:40 UT, accompanied by **loop ejections** to the south and east. From 09:32 UT onwards the loop structures are different. The **northern loops** continue to brighten and then, at about 10:00 UT, we see the onset of brightening in the **flare arcade** region. This marks the beginning of our third development stage.

In this third stage we see the ejection of a **narrow loop** structure, beginning at about 10:03 UT. Its trajectory follows the earlier **loop ejections** to the southeast, but over a much narrower angular range. We show this in Fig. 8. The structures along the **neutral line** began brightening during

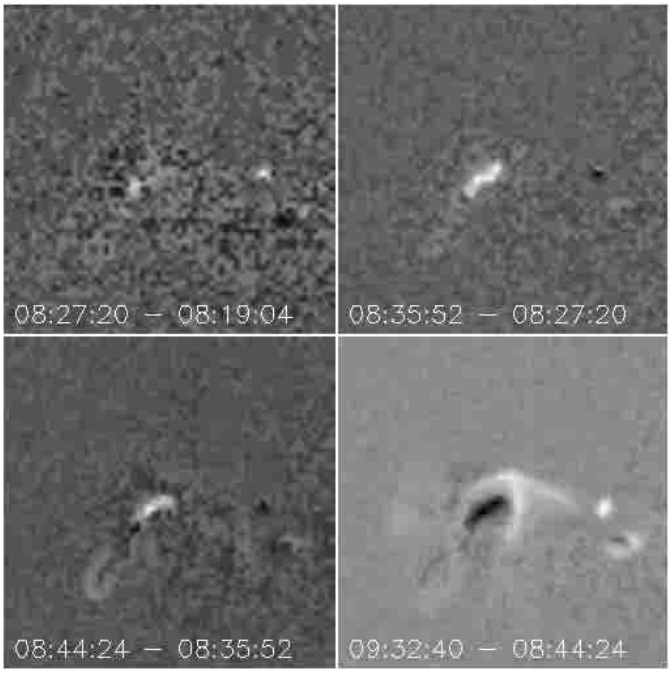

Fig. 5. Four *Yohkoh*/SXT difference images from the first activation stage of the flare development, made using the AlMg filter with 10″ pixels. The cadence is low but the images reveal brightening along the **neutral line** (see Fig. 2) that is to flare later on. In addition the **northern loops** begin to brighten during this stage.

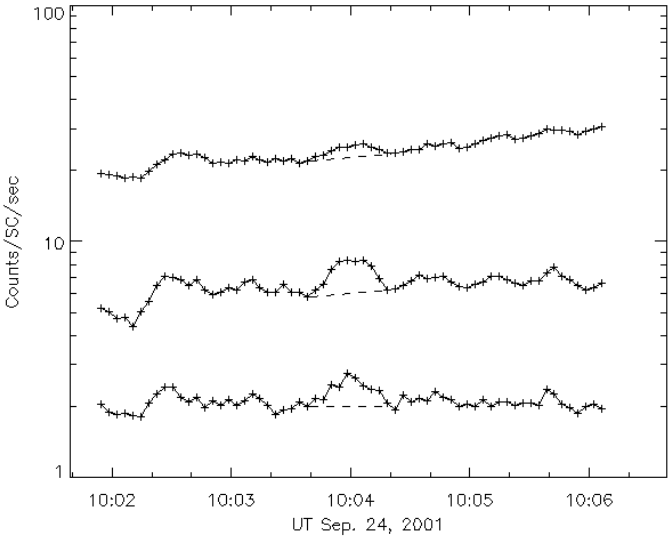

Fig. 6. Hard X-ray counts from HXT in its lowest three bands, nominally 14–23 keV, 23–33 keV, and 33–53 keV, around 10:04 UT. The dashed lines show the background levels adopted for the spectral estimate discussed in the text. The presence of counts as high as the *M*2 band, together with the short time scale, implies a non-thermal process.

this ejection, and continued until the end of soft X-ray imaging at about 10:14 UT (after this time there are no SXT images available).

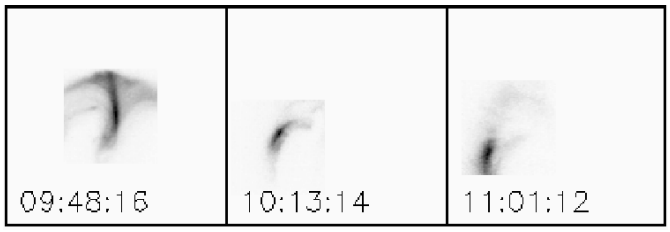

Fig. 7. Soft X-ray images from *Yohkoh*/SXT during the initial and gradual phases of the October 24 flare (thus omitting the impulsive phase, which was not observed by *Yohkoh*. The left panel shows the pre-flare active region, the middle the initial flare development, and the right the early post-flare loops (flare maximum). One can see a close match between the images from flare onset and from flare maximum.

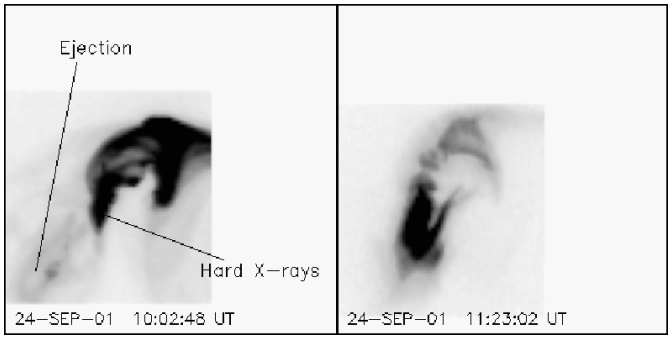

Fig. 8. Early and late soft X-ray images at 5″ pixel size, somewhat saturated. The image on the left shows the structure that became the **narrow loop ejection**, prior to its motion to the SE away from the site of the hard X-ray source. On the right one sees the bright arcade, which includes the region of the pre-flare loops seen in the first frame of Fig. 7.

3.3. Hard X-ray images and spectra

The hard X-ray variability in the activation stages of this flare strongly suggest non-thermal particle acceleration. Table 2 shows spectral estimates for the event at 10:04 UT. Here "slope" refers to the power-law spectral index γ in $F_{h\nu} = A(h\nu)^{-\gamma}$ photons $(\mathrm{cm}^2\ \mathrm{s\ keV})^{-1}$, as fit to the counting rates of adjacent channels (Sato et al. 1998). Because of the weakness of this event during the initial phase, the determination of the background counting rates is uncertain, and this systematic error dominates the estimates.

We note that the *M*2 band excess is only about 25% of the background rate at peak time. However we believe that the spectral estimates point clearly to a non-thermal bremsstrahlung model; the channel ratios (shown for adjacent pairs of channels in Table 2) are formally inconsistent with thermal models in any plausible temperature range, say below 6×10^7 K.

Overlays of hard and soft X-ray images (Fig. 9) show that the hard X-ray brightening at 10:04 UT occurred in or close to the soft X-ray loops forming at that time. The hard X-ray contours cannot be interpreted in detail (the minimum contour in each frame shown is 50%) because of errors introduced by low counting rates and ambiguous background selection. The HXT image reconstructions can depend sensitively upon data selection for background corrections, and to obtain these images we

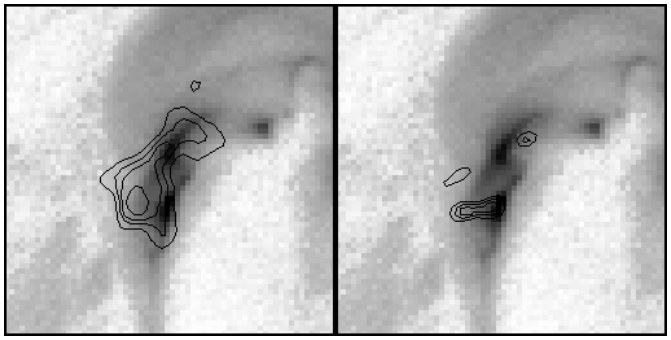

Fig. 9. Soft and hard X-ray images from the time of the 10:04 UT event shown in Fig. 6. Left, SXT image in the AlMg filter at 10:03:52 UT with 13–23 keV hard X-ray contours superposed; right, same image with 23–33 keV contours. The images are 2′29″ (114 Mm) across and have N up, W to the right. The minimum hard X-ray contour is 50% of peak brightness in each case.

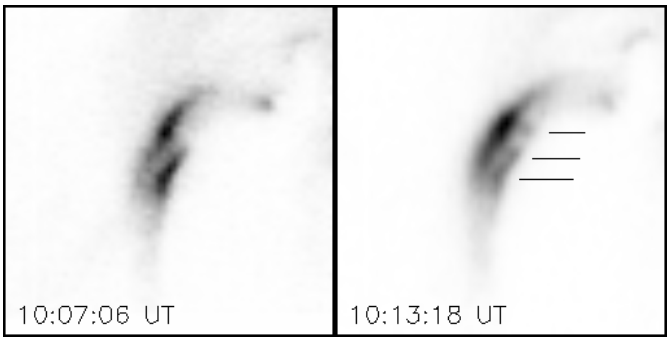

Fig. 10. Individual images of the soft X-ray loops (4.7 msec exposure through the AlMg analysis filter of SXT) during the flare onset. The lines in the image on the right indicate small temporary brightenings apparently occurring along the southern loop.

Table 2. Hard X-ray spectrum at 10:04 UT.

HXT	Channel	HXT Counts	Spectral Index
L:	13–23 keV	1.26	
M1:	23–33 keV	1.02	3.3
M2:	33–53 keV	0.25	5.5

have used the slowly-varying flare background rather than an absolute level.

Light curves made from soft X-ray images also show evidence for small-scale temporal variability. In the time range 10:07:06 UT to 10:13:42 UT there were 33 images in the AlMg filter at full resolution (one each 12 s). The images show two nearly parallel loops, as seen in Fig. 10, with their concavities in the SW direction. During this time both loops were steadily increasing in brightness, the upper one more slowly. The loop shape is inconsistent with that of a simple loops in a vertical plane, since in that case the direction of concavity should lead towards Sun center, to the NW from this flare at (S16, E23). The elongated features could also represent multiple loops blurred together, and in fact the particular image shown in Fig. 10 (AlMg from 10:13:18 UT) shows several subordinate brightenings in the southern **flare arcade** region, as marked with lines on the figure. Although these structures appear loop-like, on the basis of this variability and the general morphology we believe them to be lines of footpoints. We have no explanation for the absence of bright loops interconnecting them, nor for the fact that they do not appear to straddle the **neutral line** properly (see Fig. 2).

3.4. Densities inferred from soft X-rays

The SXT images can be converted into estimated density maps. We have done this for an image pair in the AlMg/Be119 filter pair (see Tsuneta et al. 1991) taken at 10:07:12 UT and 10:07:14 UT respectively. These filters were not available at 10:04 UT because *Yohkoh* was in its medium-rate telemetry mode. We also need to assume a line-of-sight depth to convert the soft X-ray emission measures to densities, and for this purpose we have assumed depth $D = 5 \times 10^8$ cm. The result depends on $D^{1/4}$, so a different assumption will not distort the resulting density map greatly. We show the results in Fig. 11, with contour levels at multiples of 2×10^{10} cm^{-3}. These are densities comparable to those required for the decimeter emission, and so we believe that the decimeter sources lie near the observed soft X-ray loops.

3.5. Yohkoh BCS data

We have analyzed all the spectra available (i.e. S xv, Ca xix, Fe xxv and Fe xxvi) and have confirmed some of our ideas regarding the processes occurring in the different stages of flare development. The BCS instrument does not provide useful information for the impulsive phase because of saturation. During the first stage, i.e. nearly two hours before the main peak, S xv spectra between 08:20 and 08:36 UT show that a shorter-wavelength feature was becoming more prominent. Short wavelengths either indicate emission from a blueshifted component, or show the presence of another source further south on the Sun. Unfortunately we cannot unambiguously locate this earliest stage of the emission and do not know whether it is related to the later stages physically.

At later times the S xv, Ca xix, and Fe xxv channels of BCS all show the activation stage after about 09:20 UT, but with limited data coverage. Generally the data show a gradual increase of fitted temperature, together with a more sudden increase of turbulent velocity from about 09:55 UT, correlated with the hard X-ray increase. The gradual temperature increase confirms that the gradual increase of the GOES apparent temperature (Fig. 1) does indeed represent an initial activation stage.

3.6. SOHO/EIT and Hα observations

To obtain a complete view of the event we also studied XUV and optical (Hα) images (Hα data from the Catania Observatory). From Hα data we find that during the flare a small filament disappeared. The time resolution and quality of the data available does not allow us to obtain precise information. Making difference images from the SOHO/EIT observations in the 195 Å line, we find clear manifestations

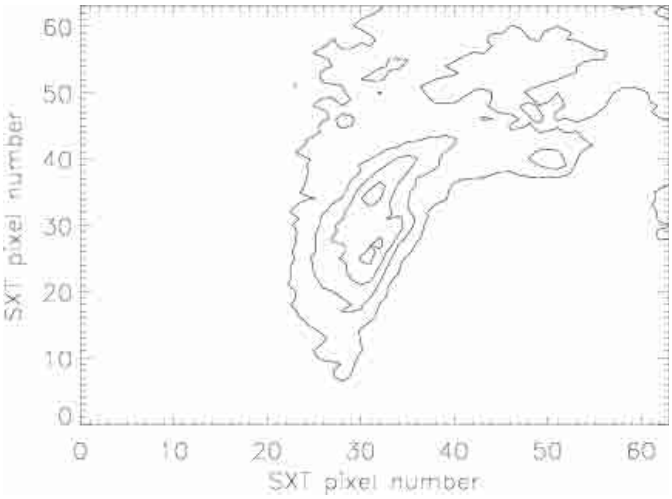

Fig. 11. Estimated density map derived from the SXT images at 10:07:12–14 UT, assuming a line-of-sight depth of 5000 km and adopting the observed temperature of 1.0×10^7 K. Contours are multiples of 2×10^{10} cm^3.

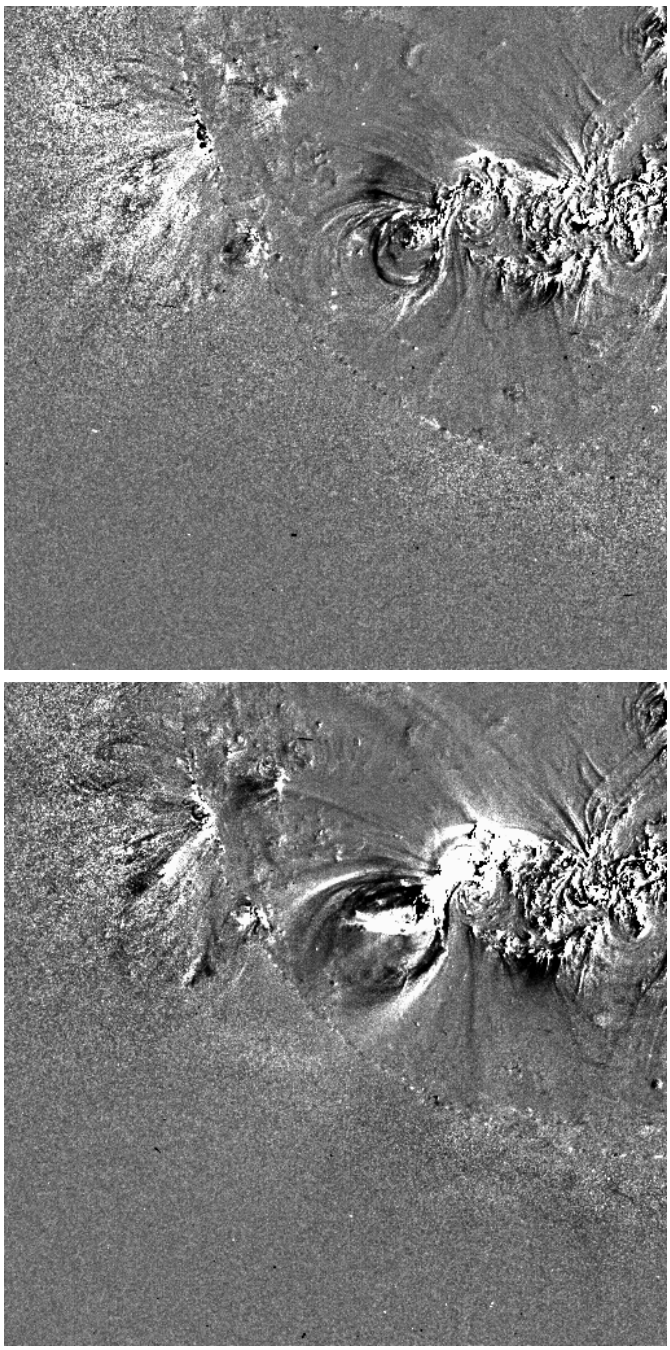

Fig. 12. Difference images derived from the SOHO/EIT observations in 195 A line. The first image was received by the differencing two XUV images taken at 09:24 and 09:36 UT, the second one at 10:00 and 10:14 UT. Expanding loops corresponds to the radio source observed by Nançay radioheliograph.

of expanding loops (see Fig. 12). These are in positions corresponding to the radio source observed by Nançay radioheliograph on frequencies 327 and 164 MHz during the flare initial phase (see next section) as well as the soft X-ray observations (Fig. 8). In addition to this, an extremely fast (~2400 km s^{-1}) halo CME appeared, with a first LASCO observation time of 10:30:59 UT.

3.7. Radio observations

This event was well-observed by the Ondřejov, Potsdam and WAVES/WIND spectrometers in a broad range of radio frequencies. Radio observations show interesting pre-flare processes starting at 9:22 UT, i.e. 55 min before the flare impulsive phase and corresponding with the hard X-ray increase at the beginning of the second activation stage (see Fig. 3). Spectral observations showed fast-drift bursts at 9:22:10–9:23:00 UT in the 0.8–1.3 GHz frequency range, see Fig. 13, and they were followed by an unusual drifting radio continuum at 9:24–10:17 UT in the 400–40 MHz frequency range (see Fig. 14). This drifting continuum is accompanied by several metric as well as interplanetary type III bursts observed by the WAVES/WIND spectrograph (see Fig. 16). The frequency drift of the drifting continuum is −0.1 MHz s^{-1} in the whole 40–400 MHz frequency range. At the same times the Nançay radioheliograph shows 327 and 164 MHz radio sources at positions southeast of the flare hard X-ray sources (in the direction of the **loop ejections** observed by SOHO/EIT at 9:36 UT (Fig. 12) and the **narrow loop** observed by *Yohkoh*/SXT (Fig. 10). Later on (10:00–10:17 UT), but still prior to the flare impulsive phase, a new group of weak fast-drift bursts with reverse slope (i.e. moving to higher frequencies) appeared in the 0.8–2.0 GHz range (Fig. 15). The time profiles show some correlation with the hard X-ray emission. Because these radio bursts are limited only to the high frequency radio range and they have a positive frequency drifts of about 130 MHz s^{-1}, we suggest that these bursts originate in closed magnetic field structures.

As shown in Fig. 15, the decimeter band reveals a swarm of fast-drift bursts prior to the main impulsive phase at about 10:18 UT. It is natural to ask if the time variability resembles that observed in soft and hard X-rays and described above. Unfortunately, as shown also in Fig. 15, there is no detailed one-to-one correlation, although there are strong coincidences (e.g. for the 10:04 UT event) shown in Fig. 15 and discussed

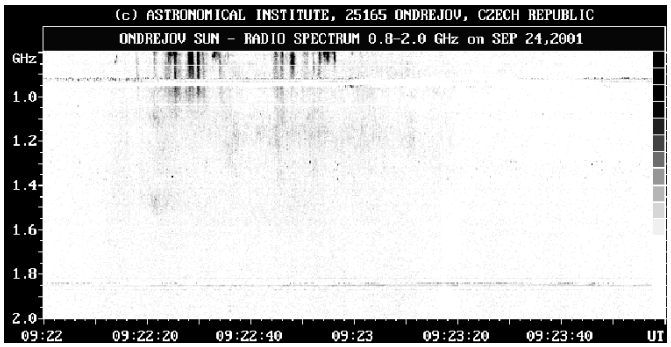

Fig. 13. The 0.8–2.0 GHz dynamic spectrum from Ondřejov showing fast drifting bursts at 09:22–09:23 UT. The emission is black.

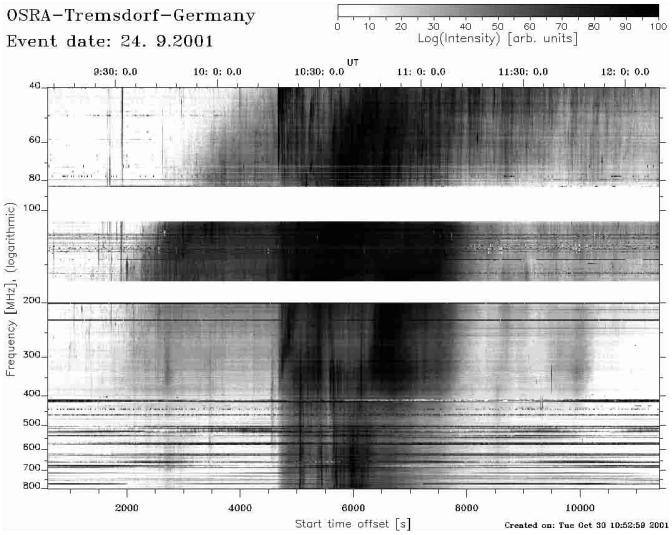

Fig. 14. The 40–800 MHz dynamic spectrum from Potsdam-Tremsdorf showing unusual drifting continuum at 09:24–10:17 UT (courtesy Dr. A. Klassen). The emission is black.

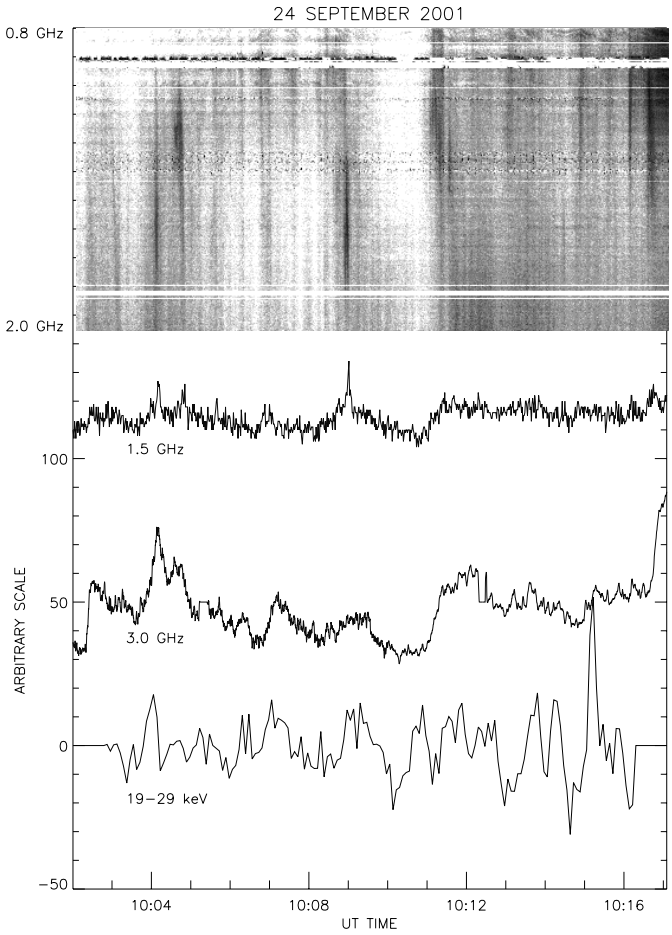

Fig. 15. Dynamic spectrum from Ondřejov, 0.8–2.0 GHz, for the early development of the September 24 flare. The fine vertical streaks (fast-drift bursts) correspond to densities 1–4 $\times$ 10^{10} cm^{-3} on the plasma-frequency fundamental hypothesis (upper part). Light curves for the radio flux at 1.5 GHz and 3.0 GHz and the HXRS hard X-ray flux in the 19–29 keV band (lower part). The X-ray flux was high-pass filtered by subtracting the values smoothed in a 200-s window. There are obvious discrepancies in the comparison, but there are also obvious correlations (for example, the event at 10:04 UT discussed above)

above. The data are too marginal for us to distinguish between flare-like brightenings, with a well-understood relationship between non-thermal and thermal effects, and some other process (as suggested for example by Warren & Warshall 2001) that may be happening in the early development of flare ribbons.

4. Discussion and conclusions

Summarizing the available observations we conclude that the flare process itself started at least as early as the beginning of the activation stage at about 09:20 UT, about an hour before the impulsive phase. Earlier soft X-ray brightenings also occurred along the **neutral line**. Counting this stage, the activation of the flare seemed to proceed in three stages, the second of which included an ejection that we associate with a filament disappearence.

In the radio range complex activity occurred at all wavelengths in conjunction with the long-duration hard X-ray emission. At longer radio wavelengths this activity often took the form of type III bursts, clear signatures of particles having access to open field lines. The filament eruption itself may have been detected as a drifting continuum source in this phase, an unusual phenomenon, and involved non-thermal electrons generated apparently in the eruptive process. We emphasize that these type III bursts extended into the hectometric band (Fig. 16), indicating that open magnetic field lines from the active region were present during the flare activation and possibly played a role in the process.

The later activation stage also involved decimetric type III emission, some of which could be temporally associated with hard X-ray emission (e.g. the small event at 10:04 UT). This involved deep atmospheric layers that could be identified with the flare by comparing density estimates, including closed magnetic field structures, as documented by a group of reverse-drift bursts at 10:00–10:17 UT in the 0.8–2.0 GHz range. No simple one-to-one time coincidence between dm reverse-drift bursts and hard X-ray peaks was found. This independence probably reflects the difference of emission mechanisms; the radio flux depends nonlinearly on the electron distribution function in velocity space, whereas the hard X-ray flux is simply proportional

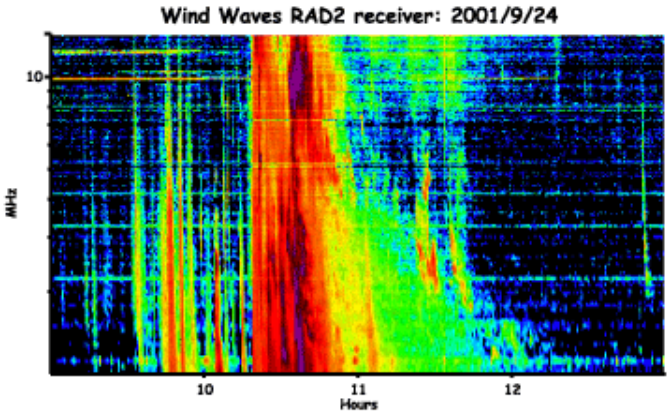

Fig. 16. Low-frequency spectrogram from the WAVES experiment on board the WIND spacecraft, consistent with an extension of the decimetric fast-drift structures to the longest wavelengths. Time scale is in hours (UT) and frequency scale from 1 to 12 MHz.

to the electron flux. We conclude that small-scale non-thermal processes, including the acceleration of electrons to typical impulsive-phase spectra in the range 10–100 keV, preceded the impulsive phase of this flare. This is not unexpected, since we know of the phenomenon of filament activation prior to the flare impulsive phase or CME acceleration time. These observations clearly link this kind of phenomenon to the possibility of particle acceleration, as revealed by the hard X-ray brightenings and by the fast-drift radio bursts.

Finally and most interestingly, the long-wavelength data show that the fast-drift bursts extend into the interplanetary medium, implying the participation of open field lines in the non-thermal activity related to the early flare development. This requirement has no counterpart in either "tether-cutting" (Moore & Roumeliotis 1992; Canfield & Reardon 1998) or "breakout" (Antiochos et al. 1998) reconnection models for flare initiation. Neither of these scenarios incorporates open field lines prior to the flare occurrence or as a part of the triggering of energy release.

Acknowledgements. The authors thank Dr. A. Klassen for the Potsdam-Tremsdorf radio spectrum, the WIND/WAVES experiment team for the WAVES spectrum, the Catania observatory for their Hα observations, and the Nançay Radioheliograph for radio images. Dr. J. Khan helped with discussion and a review of the *Yohkoh*/BCS spectral observations. NASA supported the work of H. Hudson under contract NAS8-40801. The work of F. Fárník and M. Karlický was supported by the grants of the GA of the Czech Republic (GACR) Nos. 205/02/0980 and IAA 3003202 under the Key Project of the Astronomical Institute No. K2043105 as well as by JSPS in the frame of the Czech-Japan scientific collaboration.

References

Antiochos, S. K. 1998, ApJ, 502, L181
Canfield, R. C., & Reardon, K. P. 1998, Sol. Phys., 182, 145
Dennis, B. R., & Zarro, D. M. 1993, Sol. Phys., 146, 177
Gaizauskas, V. 1989, Sol. Phys., 121, 135
Hudson, H. S., & McKenzie, D. E. 2000, Earth Planets Space, 53, 581
Fárník, F., & Savy, S. K. 189, Sol. Phys., 183, 339
Fárník, F., Garcia, H., & Karlický, M. 2001, Sol. Phys., 201, 357
Kahler, S. 1979, Sol. Phys., 62, 347
Machado, M. E., Moore, R. L., Hernandez, A. M., et al. 1988, ApJ, 326, 425
Moore, R. L., & Roumeliotis, G. 1992, in Eruptive Solar Flares, ed. Z. Švestka, B. V. Jackson, & M. E. Machado, Lecture Notes in Physics, 399, 69
Sato, J., Sawa, M., Masuda, S., et al. 1998, The Yohkoh HXT Image Catalog, Nobeyama Radio Observatory
Tappin, S. J. 1991, A&A, 87, 277
Tsuneta, S., Acton, L., Bruner, M., et al. 1991, Sol. Phys., 136, 37
Vršnak, B. 1989, Sol. Phys., 120, 79
Warren, H. P., & Warshall, A. D. 2001, ApJ, 560, L87
Webb, D. F. 1985, Sol. Phys., 97, 321